Genomic mapping identifies multiple therapeutic pathways in malignant mesothelioma

Authors:

Anca Nastase[1¶], Amit Mandal[1¶], Shir Kiong Lu[1], Hima Anbunathan[1], Deborah Morris-Rosendahl[1,2], Yu Zhi Zhang[1,3], Xiao-Ming Sun[4], Spyridon Gennatas[1], Robert C Rintoul[5,6], Matthew Edwards[2], Alex Bowman[3], Tatyana Chernova[4], Tim Benepal[7], Eric Lim[8], Anthony Newman Taylor[1], Andrew G Nicholson[1,3], Sanjay Popat[9,10], Anne E Willis[4], Marion MacFarlane[4], Mark Lathrop[11], Anne M Bowcock[1], Miriam F Moffatt[1,*], William OCM Cookson[1,*]

Affiliations

[1] National Centre for Mesothelioma Research, Imperial College London, UK

[2] Clinical Genetics and Genomics, Royal Brompton and Harefield NHS Foundation Trust, London, UK

[3] Department of Histopathology, Royal Brompton and Harefield NHS Foundation Trust, London, UK

[4] Medical Research Council Toxicology Unit, University of Cambridge, Cambridge, UK

[5] Department of Thoracic Oncology, Papworth Hospital, Cambridge, UK

[6] Department of Oncology, University of Cambridge, Cambridge, UK

[7] Department of Oncology, St George's Healthcare NHS Foundation Trust, London, UK

[8] Department of Thoracic Surgery, Royal Brompton and Harefield Foundation Trust, London, UK

[9] Department of Medicine, Royal Marsden Hospital, London, UK

[10] The Institute of Cancer Research, London, UK

[11] Department of Human Genetics, McGill University-Génome Québec Innovation Centre, Québec, Canada

[¶] Contributed equally to this study

***Corresponding authors:**

Professor William OCM Cookson: w.cookson@imperial.ac.uk; Professor Miriam F Moffatt: m.moffatt@imperial.ac.uk

Abstract

Malignant pleural mesothelioma (MPM) is an aggressive malignancy associated with asbestos exposure. It shows limited responses to all treatments. Although 20% of tumours may transiently regress after checkpoint immunotherapy[1,2], predictors of response are unknown. The molecular landscape is of low complexity but recurrent lesions have not yet defined effective therapeutic targets. In order to comprehensively map genomic alterations, we combined copy-number analysis from SNP arrays with targeted sequencing of tumours from 121 patients. We found previously unrecognised deletions in the tumour suppressor *RB1* in 26% of cases. These combined with *CDKN2A* and *TP53* lesions affected the RB tumour suppressor pathway in 65% of tumours. We show here therapeutic avenues downstream of *RB1* by finding micromolar half maximal inhibitory concentrations (IC_{50}s) of PLK1, CHEK1 and Aurora Kinase inhibitors in MPM cell lines. Non-overlapping defects in Hippo pathways (*RASSF7* amplification, *NF2*, *LATS1* and *LATS2* mutations) were present in 48% of tumours, accompanied by micromolar IC_{50}s to the YAP1 inhibitor Verteporfin. Loss of a 240Kb locus containing *SUFU* was observed in 21% of tumours, accompanied by disordered expression of Hedgehog pathway genes. *SUFU* depletion was reproducibly associated with reduced transcription of T-cell and macrophage regulators, and increased transcription of the immune checkpoint inhibitor VISTA. In half of all MPM, *CDKN2A* deletions were accompanied by loss of Interferon Type I genes. The presence of dysregulated Hedgehog immune transcription and loss of Type I Interferons indicate novel approaches to immunotherapy.

Introduction

The pleura consist of single layers of mesothelial cells that line the surface of the lungs and the adjacent chest wall. Once inhaled, insoluble asbestos fibres encourage inflammation and fibrosis, normally adaptive responses that seal off foci of injury. Within mesothelial cells however, fibres induce reactive oxygen species and double strand DNA breakages[3].

The latency of 20 to 50 years between asbestos exposure and disease means that MPM incidence is peaking in western societies that banned asbestos during the late 20th century. MPM causes 2,500 UK deaths a year and there will be a further 50-60,000 estimated cases by 2050. Global mesothelioma deaths are estimated to be 38,400 each year[4].

MPM is classified histologically into epithelioid, biphasic (mixed) and sarcomatoid subtypes. Epithelioid histology accounts for most cases and has a slightly better prognosis[5]. MPM grow remorselessly within the thoracic cavity, with metastasis usually late and uncommon. Intense accompanying fibrosis is a major cause of pain and dyspnoea.

Previous genomic analyses of MPM have shown a mutational landscape dominated by loss of function mutations in *BAP1* and *NF2*[6,7]. Larger structural variations in MPM are common[8], and recurrent

deletions are recognised for *CDKN2A* (located at chromosome 9p21.3), *NF2* (22q12) and *BAP1* (3p21.3).

Given the proclivity for asbestos to induce DNA damage, we extended genomic findings in 121 MPM tumours by fine mapping of copy-number alterations (CNAs) with high density SNP arrays. We explored the mutational spectrum with whole exome sequencing (WES) in 50 subjects (21 of which had paired blood samples for germline DNA), before extending mutation detection to all tumours with a 57-gene targeted capture next-generation sequencing (TC NGS) panel (Extended Data: Figure 1a,b and Extended Data: Table3).

Results

Demographic and clinical characteristics

One hundred and five of the 121 patients (87%) were male (Extended Data: Table 1). Ninety tumours exhibited the epithelioid subtype, 25 were biphasic and 6 were sarcomatoid (Extended Data: Figure1c). Patients with sarcomatoid disease were older than the other two groups. Asbestos exposure had been documented clinically in 69% of cases. Survival time from diagnosis to death or last follow-up was available for 110 patients. The median overall survival (OS) for all subjects was 9.9 months with sarcomatoid patients showing a worse outcome than others (Extended Data: Table 1 and Figure 1d).

Copy number alterations (CNAs)

We analysed >950K SNPs (Illumina Infinium OmniExpressExome-8 v1.3 and v1.4) for CNAs using the GISTIC program. The latter estimates genomic boundaries for recurrent CNA events and assigns statistical significance after false discovery rate (FDR) corrections[9].

Deletion of *CDKN2A* was detected in 71/118 tumours (60%): 58 (82%) deletions were predicted homozygous (Figure 1a and Figure 2). As previously reported[6,7], *CDKN2A* loss was associated with worse OS than other lesions (8.8 vs 13.0 months, Kaplan-Meier P=0.02) (Figure 1c).

Deletion of the *CDKN2A* region is extensive in many malignancies, and a full locus map (Figure 1b) revealed large deletions to also be present in MPM. The map showed a frequent but previously unreported loss of the closely neighbouring Type I Interferon genes (Figure 1b): 38/118 (32%) patients had predicted homozygous *IFN* loss and 24/118 (20%) had heterozygous loss.

We observed frequent deletions at multiple other loci (Figure 1d-f, Extended Data: Table 2). Novel deletions included the *RB1* locus on 13q14.2 in 31/118 patients (26%). The *RB1* tumour suppressor is activated downstream of CDK4 and CDK6[10].

Loss of a locus on 10q24.32 containing *SUFU* (*Suppressor of Fused)* was observed in 25/118 tumours (21%). *SUFU* inhibits activation of GLI transcription factors in the Hedgehog pathway, which is disordered during MPM carcinogenesis[11,12].

Previously unrecognised regions of amplification (Figure 1a and Figure 2, Extended Data: Table 2) included a locus on 11p15.5, amplified in 39/118 tumours (33%) and containing *RASSF7* and *miR-210* (Figure 1g). When up-regulated *RASSF7* controls cell growth and apoptosis in different tumours[13], and functions as an oncogene in non-small cell lung cancer (NSCLC) interacting with *MST1* to inhibit Hippo signalling[14].

Other substantial amplifications included 19q13.43 in 24/118 tumours (20%), containing *NLRP5*, *ZNF444* and *ZNF787*; 5q35.2 in 27/118 tumours (23%), containing *GPRIN1* immediately adjacent to *CDHR2* which may moderate contact inhibition of epithelial cells[15]; and 5q35.3 in 26/118 tumours (22%) containing *LTC4S* and *SQSTM1*. The latter encodes p62, a mediator of autophagy influencing tumorigenesis, malignant growth and resistance to therapy[16].

Somatic mutations

WES in 50 tumours (21 with paired peripheral blood DNA (PBL)) revealed no major loci beyond those previously described[6,7]. We completed TCS in 119 patients, 77 of which had PBL, achieving a mean coverage of 792X for tumours and 802X for PBL. *BAP1* was mutated in 39 subjects (33%); *NF2* in 24 subjects (20%); *TP53* in 9 subjects (8%) and *SETD2* in 7 subjects (6%) (Figure 2 and Extended Data: Figure 2). Mutations were scattered across these coding regions of the genes (Extended Data: Figure 3 b-d), consistent with their putative role as tumour suppressors.

We found two *NRAS* mutations at known oncogenic RAS hotspots (G12V and Q61H). Three other RAS pathway related genes were identified by WES: a *NF1* stop mutation (c.6439C>T, p.Q2147*), a splice site *RASA1* mutation (c.829-1_858.del) and a *HRAS* in-frame deletion (c.187_189del, p.E63del).

TP53 mutations carried a worse prognosis than other mutations (mean OS 5.7 vs. 13.6 months, P=0.0005), as previously described[6]. We did not detect significant associations of other mutations with age or survival.

Combined analysis of CNA, WES and TCS (Figure 2) showed *CDKN2A* deletion to be present in 60% of tumours; *BAP1* mutated or deleted in 54%; *RASSF7* amplification in 33%; *RB1* deleted or mutated in 26%; *NF2* mutated in 20%; *TP53* mutated in 8%; *SETD2* in 6%; *DDX3X* in 5% and *LAST2* in 5%.

Germline mutations

We detected a missense germline mutation localized in the UCH domain of *BAP1* from one patient with epithelioid subtype (Extended Data: Figure 3b). In other subjects, single deleterious germline mutations were found in *MSH5* and *MSH6* (representing the mismatch-repair (MMR) pathway), *RB1*, *SETD6* and *BRCA2*.

Mutational burden and signatures

We found a median of 31 non-synonymous somatic mutations per tumour in the 21 WES paired samples, consistent with the low rate observed by Bueno *et al*[6]. In the targeted capture where we had

77 paired samples available, we again observed low tumour mutational burden (Extended Data: Figure 3i). One patient (NCMR033) had a hypermutated tumour (167 somatic mutations), accompanied by the frame-shift deletion in *MSH6* (p.Phe1104LeufsX11) and a frame-shift insertion in *PALB2* (p.Met1049AspfsX4), encoding a protein that recruits BRCA2 and RAD51 at the site of double-strand breaks[17].

The mutation spectrum was characterized by C>T transitions, in both WES and TCS panel data (Extended Data: Figure 3e and a respectively), consistent with earlier reports[6,7]. Analysis of mutational signatures[18,19] found COSMIC signatures 3, 6 and 15 to be prevalent in the 21 paired WES samples (Extended Data: Figure 3e, f) and in WGS from 19 primary low passage MPM cell lines[20] (Extended Data: Figure 3g, h).

Signatures 3, 6 and 15 are all indicative of DNA damage and breakpoint repair[19]. In other cancers, signature 3 mutations accompany biallelic inactivation of *BRCA1* or *BRCA2*, where the inability to repair DNA predicts good responses to platinum therapy. MPM responds poorly to such therapies, and we hypothesise that signatures of DNA damage may follow the actions of asbestos in the progenitor neoplastic cell.

These results and the remarkable consistency of genetic lesions in MPM in humans and in mice[21,22] suggest a hypothesis that recurrent MPM breakpoints and mutations occur in regions of chromatin that have been opened in response to asbestos. Indeed, *Cdkn2a* loss and Hedgehog and Hippo pathway activation have been observed in murine models of asbestos exposure well before tumour development[11,21,22].

Histology

We did not see any significant associations between common lesions and histological subtypes in the full dataset. However, RNA sequencing (RNASeq) revealed differential transcription between subtypes (Extended Data: Table 4). As reported previously[6], *WNT5B* had higher expression in the sarcomatoid subtype. Other genes significantly upregulated ($P_{adjusted}$<0.001) in non-epithelioid tumours included *GPR176* which acts as a circadian pacesetter[23], and known adverse factors for other cancers such as *IGF2BP1*, *CCBE1*, *HS3ST3A1*, *TRAM2* and *SERTAD2*.

We tested how the most frequent genomic alterations, *BAP1* mutation and *CDKN2A* deletion, were translated at protein levels by staining 28 tumours (Extended Data: Figure 4a) with antibodies against BAP1 and MTAP (as a potential surrogate marker for *CDKN2A* deletion) (Extended Data: Figure 4d,e).

BAP1 staining revealed general or focal loss in 17/28 (61%) of the analysed cases, which partially associated with *BAP1* mutation or deletion (*P*=0.01) (Extended Data: Figure 4f). There was significant association when comparing MTAP H-score between *CDKN2A*/*MTAP* deleted and wild-type samples (*P*=0.001) (Extended Data: Figure 4g). The mitotic count and Ki-67 (both indicators of proliferation)

correlated with each other (*P*<0.0001, r=0.42). Ki67 correlated with copy number burden (*P*=0.03, r=0.42) and with MTAP score (*P*=0.04, r=0.39), consistent with disordered cellular division accompanying *CDKN2A* loss.

Identifying genomic vulnerabilities in MPM

We explored potential therapeutic pathways by determining the half maximal inhibitory concentration (IC_{50}) of selected compounds with three patient-derived low passage (<15) primary MPM cells[20] that had been whole-genome sequenced and targeted protein were tested by western blot (Figure 3a). For comparison, we included an immortalized mesothelioma cell line (H2052), a lung adenocarcinoma cell line (A549), and a transformed normal mesothelial cell line (Met-5A). We exposed cells to a range of drug concentrations (0.0005 to 50 micromolar (µM)), using as controls DMSO treated cells (Figure3b-g).

DNA repair

Because of the signatures of DNA breaks, we tested two PARP inhibitors (Niraparib and Olaparib) that are effective in homologous repair deficiency[24]. Despite reports suggesting utility in MPM[25], we did not see a consistent inhibition of primary cell growth (Figure 3h).

Cell cycle and RB1

The *CDKN2A* locus encodes *INK4A* (*p16*) and *ARF* (*p14*) genes. *p16* normally restrains cyclin-dependent kinases, so that CDK4/CDK6 inhibitors are potentially therapeutic for MPM[10]. However, CDK4 and CDK6 downstream effects include phosphorylation and activation of *RB1*[10], and our finding of *RB1* deletions in 34% of tumours with *CDKN2A* loss may make responses to CDK4/CDK6 antagonists less likely.

The combination of *CDKN2A*, *RB1* and *TP53* deletions or mutations meant that 79/121 (65%) of the tumours had lesions in the RB tumour suppressor pathway. *RB1* loss has recently been shown to confer a robust and selective vulnerability to drugs that target DNA damage checkpoint (*CHEK1*) and chromosome segregation proteins such as Polo-Like-Kinase 1 (*PLK1*)[26]. *CHEK1* is over-expressed in MPM[27], and RNAi screens have shown MPM lines to be sensitive to *CHEK1* and *PLK1* knockdown. *RB1* deficient tumours are hyper-dependent on Aurora kinase B (AURKB) for survival[28], and AURKB inhibitors are efficacious against *RB1* deficient lung cancers at non-toxic doses[28].

A CDK4/CDK6 inhibitor (Palbociclib, PD0332991) showed only minor effects in our cell lines (Figure 3h). However, we found micromolar (µM) to sub-µM responses when treating with an Aurora Kinase inhibitor (Alisertib, MLN8237); an inhibitor of *PLK1/2/3* that induces G2/M arrest and apoptosis (Volasertib, BI6727)[29]; and a *CHEK1/2* inhibitor that abrogates the G2/S checkpoint (AZD7762).

Hippo signalling

Hippo monitors external factors that shape tissue structure[30]. *NF2* recruits core Hippo signalling pathway members (*LATS1/2*) to inhibit activation of the transcriptional cofactors YAP1 and TAZ[31].

RASSF7 also regulates Hippo pathways, and its overexpression promotes phosphorylation and nuclear translocation of YAP1[14]. We found *RASSF7* amplification in 39 subjects, *NF2* mutations in 24, *LATS2* mutations in 5 and *LATS1* in 3, so that non-overlapping lesions in Hippo pathways were present in 58/121 subjects (48%) (Figure 2). *WNT5B*, increased in sarcomatoid tumours, may also induce YAP/TAZ activation through non-canonical pathways[32].

We did not find significant differences in transcript abundances when comparing RNASeq for *RASSF7* amplifications to other tumours; or for lesions in Hippo signalling genes (*NF2*, *LATS1*, *LATS2)* singly or combined; or for *SETD* mutations combined. We did not detect the *RASSF7* amplification in any of 20 primary cell lines examined by SNP array, which may reflect selection in culture for MPM genotypes that grow independently of a fibroblast matrix.

Our results nevertheless support YAP1 axis inhibition for MPM therapy[31], and we found µM IC_{50} responses to the YAP inhibitor Verteporfin in all MPM cell lines (Figure 3h). Notably, Meso-27T that is not deficient in *NF2* responded, as did immortalised Met-5A mesothelial cells. Vertiporfin is in common use as a photosensitiser in the therapy of macular degeneration.

Loss of *BAP1*

When compared to other tumours, *BAP1* mutations or deletions were associated ($P_{adjusted}$<0.05) with up-regulation of the *RET* proto-oncogene[33] and *NNAT*, which is associated with poor outcome in multiple cancers[34] (Extended Data: Table 6). We found the negative association of *BAP1* with *RET* to be present also in the Bueno *et al*.[6] (r=-0.32, *P*=2.2E-06) and TCGA-Meso[7] (r=-0.45, *P*=1.3E-06) datasets. The results suggest tumour suppressor activities of BAP1 beyond deubiquitination[35]. It may be of interest that RET inhibitors are effective in RET-driven NCSLC and thyroid cancers[36].

Hedgehog signalling

Loss of the *SUFU* locus in 21% of tumours (21.2%) were associated with marked upregulation of the *Patched 2* tumour suppressor (*PTCH2*) (Table 1). *Ptch2* overexpression has been observed in *Sufu* knockout mice and is indicative of aberrant Hedgehog signalling[12]. Hedgehog pathways are activated in MPM patients, in the absence of obvious mutations[11]. Also upregulated were *NHS*, *HOXA7* and *TRPS1*, each of which regulate tissue differentiation (Table 1).

We found a SMO (Smoothed) inhibitor (Vismodegib, GDC-0499) to be inhibitory in one MPM cell line (Figure 3h), although Hedgehog inhibition may be most effective in modulating tumour and stromal interactions[37] that should be investigated in organoid or murine models.

SUFU loss unexpectedly correlated with downregulation of prominent T-cell genes (Table 1), including *ODF3B*; the killer-cell receptor *KLRD1* (*CD94*); and *HSH2D*, a target of T-cell activation. Downregulated monocyte/macrophage and dendritic cell markers included *IL4R*, *SCIMP*, *SIGLEC1* (*CD169*), *CLEC10A*, and *CR1* (Complement C3b/C4b receptor 1).

We confirmed these results in independent datasets from Bueno *et al*.[6] and TCGA-Meso[7], finding that abundances of Hedgehog pathway transcripts *SUFU*, *PTCH1* and *PTCH2* correlated with *KLRD1* and *CR1* (Extended Data: Table 5).

These findings extend to malignancies with known central function of Hedgehog signalling in T-cells at the immunological synapse[38,39].

Immune context

Checkpoint inhibitors targeting PD-1 and its ligand PD-L1 cause marked tumour regression in some patients with MPM[2]. However, PD-L1 is expressed at a low level, if at all, in most MPM and its status imperfectly predicts response to immune checkpoint inhibitors[2].

In our tumours, IHC staining for PD-L1 was low, with only 4/28 cases (14%) ≥ 10% expression, and one case > 70%. There was a good correlation between PD-L1 (SP263) staining and transcript abundance ($P<0.01$, r=0.7) (Extended Data: Figure 4h). We did not see a consistent relationship between any Hedgehog-related transcripts and PD-L1 (Extended Data: Table 5).

High-level staining of the alternative immune-checkpoint protein VISTA (V-domain Ig suppressor of T cell activation)[40] has been observed in epithelioid MPM, and implies a better prognosis[7,41]. We confirmed a high level of VISTA by IHC in our samples (Extended Data: Figure 4), and in RNASeq data replicable associations were seen between VISTA and *SUFU*, *PTCH1*, *PTCH2*, *KLRD1* and *CR1* (Extended Data: Table 5). These findings provide a stimulus to further investigate VISTA therapeutic blockade.

It may also be of interest that the Type I Interferon genes were deleted in 52% of all MPM. Interferons induce complex pro-inflammatory responses within tumour cells as well as in accessory immune cells[42,43]. Homozygous deletion of IFN genes is associated with poor response to CTLA4 blockade in patients with malignant melanoma[44]. Historically, administration of IFNA2 to patients with MPM has occasionally induced complete regression[45,46]. Additionally, early stage trials suggest that intra-pleural infection with viral vectors containing *IFNA2*[47] or *IFNB1*[48] induce inflammation and encourages beneficial responses in MPM, suggesting an adjuvant role for interferons in the therapy of MPM.

Conclusions

Our results indicate possible roles for Aurora Kinase, PLK, CHK and YAP inhibitors in the treatment of MPM growth. IFN Type I and *SUFU* deletions as biomarkers may guide more effective immunotherapies. VISTA inhibition may directly modify immune recognition of MPM, and an adjuvant role in immunotherapy seems possible for Hedgehog inhibitors. The involvement of Hippo and Hedgehog signalling and the intense fibrosis seen clinically assert a central role for tumour-matrix interactions in the pathogenesis of MPM, and suggest therapeutic avenues beyond tumour cell killing.

Methods

Sample collection

Thirty unpaired tumour samples were obtained from the NIHR-BRU Advanced Lung Disease Biobank and Royal Brompton and the Harefield NHS Trust (RBH) Diagnostic Tissue Bank (NRES:10/H0504/9 and 10/H0504/29) with eighty-two paired (tumour and blood) and 4 unpaired tumour samples obtained from MesobanK UK, Cambridge (NRES:13/EE/0169). Seven additional paired samples were obtained from the EQUALITY study (NRES:10/H0808/53). Tissues were optimally collected during diagnostic or surgical procedures prior to any anti-cancer treatment and were all snap frozen with or without RNAlater. Formalin-fixed paraffin embedded tissues were sectioned, stained with routine haematoxylin and eosin, and reviewed by two experienced pathologists to verify tumour histology and abundance. For RBH and EQUALITY tumours, tissues with 30% or more viable-appearing malignant cells were selected for whole exome sequencing (WES). MesobanK samples contained only tumours with > 50% malignant cells.

Genomic DNA isolation and quality control

Genomic DNA was isolated from frozen tumour tissues and matched normal tissue (blood) with routine methods (Qiagen DNA and RNA extraction kits, Qiagen, Hilden, Germany). DNA yield and purity were assessed with the Quant-iT™ PicoGreen dsDNA Assay Kit (Life Technologies, Carlsbad, USA) or Qubit 3.0 fluorimeter (Thermo Scientific, Massachusetts, USA) according to manufacturers` protocols.

Whole exome sequencing

WES was performed at the McGill University and Genome Quebec Innovation Centre, Canada. Genomic DNA from tumour and blood samples were fragmented and hybridised as per SureSelect^{XT} Target Enrichment System (Agilent SureSelect Human All Exon V4) for the Paired-End Multiplex Sequencing protocol. The captured libraries were sequenced on an Illumina HiSeq2000 according to standard protocols.

Targeted sequencing of a custom gene panel

The entire coding regions of fifty-seven genes were included in a hybridisation capture panel (Extended Data: Table 3), based on: recurrence in our WES tumour set; reported in the Catalogue of Somatic Mutations in Cancer (COSMIC) database; implicated in cancer[49]; or reported in the TCGA or Bueno *et al.* studies[6,7]. Sequencing libraries were prepared from DNA extracted from tumours and normal tissue (whole blood) samples using the SureSelect QXT Target Enrichment System (Agilent, Santa Clara, USA) according to the manufacturer`s protocols. Sequencing was performed on a MiSeq or NextSeq500/550 platform (Illumina) with a mean read depth of 780.6X (all samples).

Data processing and quality control

Raw fastq were quality checked before alignment with BWA mem (v 0.7.12). GATK software (v 3.8 and 4.1) was used to refine the alignment data before variant calling. For Target capture sequencing

(TCS), somatic and germline variant calling was performed for the paired samples using VarScan software (v 2.4.2). For the un-paired samples joint variant calling was performed using Platypus (v 0.8.1). In case of WES, joint variant calling was performed at McGill using the GATK HaplotypeCaller.

Detection of candidate pathogenic somatic and germline variants

Candidate somatic and germline variants were checked for presence in population data and those with frequency >=10^{-3} were deemed polymorphic and filtered out. Further selection was based on either being assigned as High or Moderate impact by VEP [50] or predicted to be splice-site altering (dbscSNV [51] score of >0.6) by at least two of three algorithms. Further prioritisation of SNV (single nucleotide variant) candidates was done based on predicted deleteriousness from any one of SIFT, Polyphen and MutationTaster algorithms.

Copy-number (CN) analysis

121 DNA samples were interrogated at Eurofins against the Human Infinium Omni-Express-Exome v 1.3 and v 1.4 Bead Chips (Illumina) arrays containing >950K markers. 118 samples remained (77 paired and 43 unpaired) after QC checks. Raw copy number data (LRR and BAF) were exported from GenomeStudio software (v 1.9.4). GC correction was performed to account for genomic 'wave artefacts affecting SNP arrays using ASCAT (v 2.4.4). The GC corrected Log R ratios (LRR) were then processed using DNACopy (v 1.52) for segmentation and filtered for marker support. Recurrent germline CN segments were identified and subtracted from the tumour sample CN segments. Germline subtracted copy number segments were then processed with GISTIC (v 2.0.23). Plotting of GISTIC results were done in maftools (v 1.4.28).

Mutation signature analysis

Somatic single nucleotide variants (SNVs) from the 21 paired WES samples were analysed for tri-nucleotide frequency around the mutated base using MutationalPatterns[52] in R. The Sanger COSMIC signature panel (n=30) was used to infer mutational processes by obtaining the percentage contribution of 30 signatures per sample. Only signatures contributing to >25% of samples were carried forward. Paired germline samples were not available for whole-genome sequencing (WGS) of 19 MPM primary cells (one MPM primary cell WGS had failed QC), and so annotation-assisted filtering of the total SNVs was done and only those SNVs that were non-polymorphic and either protein-sequence altering or predicted to be splice-site altering, were considered and analysed as described for the tumour tissue samples.

RNA sequencing

Total RNA was isolated by means of RNEasy Fibrous Midi kit (Qiagen, Hilden, Germany) according to manufacturer`s protocol from 35 tumours. Concentration and quality were determined with the 2100 Bioanalyzer and Total RNA Nano kit (Agilent Technologies, California, United States) as per manufacturer's instructions. RNA sequencing was performed at McGill.

Immunohistochemistry

3µm whole slide FFPE tumours sections mirroring fresh frozen tissue used for molecular analysis underwent H& E staining according to routine histopathological protocols. Further sections underwent staining for BAP-1 (Santa Cruz BioTechnology, clone C4), Ki67 (Ventana, 30-9), MTAP (NovusBio, 2G4), PD-L1 (Ventana, SP263) and VISTA (D1L2G, Cell Signalling Technology). Mitotic activity was evaluated by counting the number of mitotic figures in the area of highest activity, over 10 high powered fields (0.24mm^2).

Whole genome sequencing of primary cell lines

Genomic DNA extracted from patient derived MPM cell lines (n=20, of which one failed QC) and primary normal mesothelial cells, MES-F (purchased from ZenBio, USA) underwent WES (McGill) and SNP genotyping (Eurofins). Genomic details of the commercial cell line were obtained from published data (COSMIC, CCLE databases, 61).

In vitro drug testing

Patient-derived primary cells, Meso-27T, Meso-33T and Meso-70T were obtained from the MRC Toxicology Unit, University of Cambridge, UK. Commercial cell lines NCI-H2052 (sarcomatoid mesothelioma), A549 (lung adenocarcinoma) and Met-5A (normal mesothelial, SV40 transformed) previously obtained from ATCC were gifted from the MRC Toxicology Unit. Original establishment of the primary cells was as previously described[21]. All primary cells and cell lines were maintained in RPMI-1640 growth media supplemented with L-glutamine (2 mM), penicillin (100 U/ml), streptomycin (100 µg/ml) and 10% FBS at 37 °C in 5% CO_2.

Eight drugs were investigated: Niraparib (MK-4827, HY-10619, MedChem Express), Olaparib (HY-10162, MedChem Express), Palbociclib, PD0332991 (A8316, ApexBio), Alisertib (MLN8237, S1133, Selleckchem), Volasertib (BI6727, S2235, Selleckcehm), Vismodegib (GDC-0499, S1082, Selleckchem), AZD7762 (S1532, Selleckchem) and Verteporfin (SML0534, Sigma Aldrich). All drugs were diluted in DMSO and aliquots maintained at -20°C. Drug aliquots were freeze-thawed no more than three times. For all experiments, controls consisted of DMSO-alone treated primary cells or cell lines.

Cells were seeded in 96-well plates (4 x 10^3 cells/well) 24h prior to drug treatments. Each line was treated for six days (except for drug PD0332991 where treatment was 3 days) with a range of concentrations from 50 to 0.0005µM. Cell viability was measured with MTS assay (CellTiter 96® AQueous One Solution Cell Proliferation Assay, Promega) on a plate reader (Tecan).

Three independent experiments, each having three technical replicates, were conducted for each drug tested. Results are represented as the average normalized to the control at each time point (mean ± s.e.m.). Briefly, the raw optical densities obtained from each well were normalized to the average of DMSO control wells, that was considered 100% viability (maximal DMSO concentration used was

0.5%). IC_{50} values were calculated with Graph Pad Prism 5 software using a dose-response curve fit model using the nonlinear log (inhibitor) versus response-variable slope (four parameters) equation. In addition, the IC_{50} values were only considered if the software gave unambiguous results and the R^2 value was > 0.7.

Statistical analysis

Categorical variables were evaluated using Fisher's exact test for two-by-two comparison or Pearson's χ^2 for comparison that exceeded the two-by-two condition. Differences between groups were evaluated by means of nonparametric Mann-Whitney or Kruskal-Wallis test.

Clinical outcomes

Overall survival (OS), defined as time from date of diagnosis to time of death, was available for 110 patients. OS was estimated using the Cox-Mantel log-rank test, Kaplan-Meier method. Censoring of OS was done at the date of the last follow-up if death did not occur. Survival analyses were performed using the long-rank Kaplan-Meier and the differences in survival curves were assessed by Mantel Cox Log rank test. A $P \leq 0.05$ was considered statistically significant and noted as: $^{*}P \leq 0.05$, $^{**}P \leq 0.01$, $^{***}P \leq 0.001$. Tests and graphs were performed with Graph-Pad Prism 5 (GraphPad Software Inc, San Diego, CA), SPSS Statistic 25 or R studio.

Acknowledgements:

This study was financially supported by a Libor Fund grant from the UK Department of Health, and by the Asmarley Foundation. SP acknowledges NHS funding to the Royal Marsden Hospital-Institute of Cancer Research Biomedical Research Centre. We thank Cambridge Biomedical Research Centre and Cambridge Cancer Centre.

Author contributions:

WOCMC, MFM, ML, SP and AMB planned the study; AN processed samples and prepared libraries for targeted capture sequencing, post-analysed whole exome, TCS, RNA sequencing and IHC data, and performed drug testing on primary cells and cell lines; AM performed bioinformatics analysis of whole exome and whole-genome sequencing, target capture, RNA sequencing and copy number data; SG and SKL processed and prepared samples for whole exome, RNA sequencing and copy number analysis; HA analysed WES data; DMR and ME provided support in generating the TCS panel and analysis of the libraries; AB performed immunohistochemistry staining, YZZ and AGN interpreted immunohistochemistry data; TC, XMS, AEW and MM established and characterized primary cells from tumours; ML oversaw whole-exome and RNA sequencing of the samples and advised on analyses; EL, RCR and TB gathered samples and associated metadata for the study; and SP and ANT provided clinical and epidemiological scientific guidance. AN and AM wrote the first draft of the manuscript with guidance by WOCMC, MFM and AMB, before editing by all the other authors.

Competing interests statement:

The authors have no competing interests to declare. SP reports honoraria from BMS, Roche, Takea, AstraZeneca, Chugai, Novartis, Pfizer, MSD, EMD Serono, Guardant Health, AbbVie, Boehringer Ingleheim, and Tesaro.

Tables

Table 1. Genes differentially regulated with *SUFU* deletions

Log$_2$ Fold Change	Av. Exp.	*P*	*P* Adj.	Chr	Name	Description
3.66	1.95	2.23E-05	3.09E-02	1	*PTCH2*	Patched 2 tumour suppressor, indicative of aberrant Hedgehog signalling
2.82	3.91	4.61E-05	3.64E-02	13	*GJB2*	Gap junction protein beta 2
2.78	3.53	1.15E-04	4.36E-02	12	*NXPH4*	Neurexophilin 4
2.35	1.35	1.18E-04	4.37E-02	X	*NHS*	Regulates actin remodelling and cell morphology
2.32	1.77	1.12E-04	4.32E-02	7	*HOXA7*	Transcription factor regulating morphogenesis and differentiation
1.26	3.26	1.20E-04	4.38E-02	8	*TRPS1*	Transcriptional repressor GATA binding 1
1.09	2.94	4.48E-05	3.64E-02	1	*C1orf112*	Chromosome 1 open reading frame 112
-0.88	5.75	7.01E-05	3.95E-02	10	*MMS19*	Cytosolic iron-sulphur assembly component
-1.06	4.79	7.90E-06	2.85E-02	10	*ZFYVE27*	Zinc finger protein
-1.11	5.89	1.18E-04	4.37E-02	16	*IL4R*	Interleukin 4 receptor
-1.11	5.30	4.78E-05	3.64E-02	10	*ERLIN1*	Binds cholesterol and regulates SREBP signalling pathway
-1.15	4.37	1.51E-05	2.85E-02	10	*FBXL15*	F-box and leucine rich repeat protein 15
-1.18	7.24	7.23E-05	3.95E-02	10	*WBP1L*	WW domain binding protein 1-like
-1.33	4.54	3.28E-05	3.43E-02	10	*SUFU*	Negative regulator of hedgehog signalling
-1.49	6.14	1.72E-05	2.85E-02	6	*CCND3*	Regulatory subunit of CDK4 or CDK6, involved in phosphorylation Rb1
-1.51	6.19	1.10E-05	2.85E-02	3	*DTX3L*	Deltex E3 ubiquitin ligase
-1.52	5.09	6.97E-05	3.95E-02	22	*ODF3B*	Differentially regulated in pathogenic CD4(+) T cells in MS
-1.55	7.58	1.05E-04	4.20E-02	10	*MYOF*	May be involved in membrane regeneration and repair
-1.58	4.43	6.91E-06	2.85E-02	18	*EPB41L3*	Erythrocyte membrane protein like
-1.63	2.83	9.32E-05	4.11E-02	17	*SCIMP*	TLR adaptor promotes cytokine production from macrophages; involved in MHC class II signalling
-2.13	4.41	9.12E-06	2.85E-02	10	*AVPI1*	Arginine vasopressin induced 1
-2.19	5.23	2.04E-05	3.09E-02	20	*SIGLEC1*	CD169: CD169 macrophages dominate antitumor immunity by presenting dead cell antigens
-2.24	5.86	7.82E-05	3.95E-02	10	*IFIT3*	IFN-independent upregulation of IFN-stimulated Genes during CMV infection
-2.27	5.68	3.33E-05	3.43E-02	12	*OAS2*	Involved in the innate immune response to viral infection
-2.67	3.10	1.09E-04	4.26E-02	17	*CLEC10A*	Specific Marker for human CD1c+ dendritic cells: enhances TLR7/8-induced cytokine secretion
-2.73	1.58	1.39E-04	4.86E-02	12	*KLRD1*	CD4: Killer cell receptor, may be involved in the regulation of NK cell function
-2.97	1.89	1.76E-05	2.85E-02	1	*CR1*	Complement C3b/C4b receptor 1: found on dendritic and other cells
-3.08	2.61	4.28E-05	3.64E-02	19	*HSH2D*	Target of T-cell activation signals: TCR antigen recognition, and co-stimulation by CD28
-3.56	3.19	1.36E-04	4.82E-02	11	*HRASLS5*	HRAS like suppressor family member 5

Figures

Figure 1. Mapping of copy number alterations in subjects with Malignant Pleural Mesothelioma

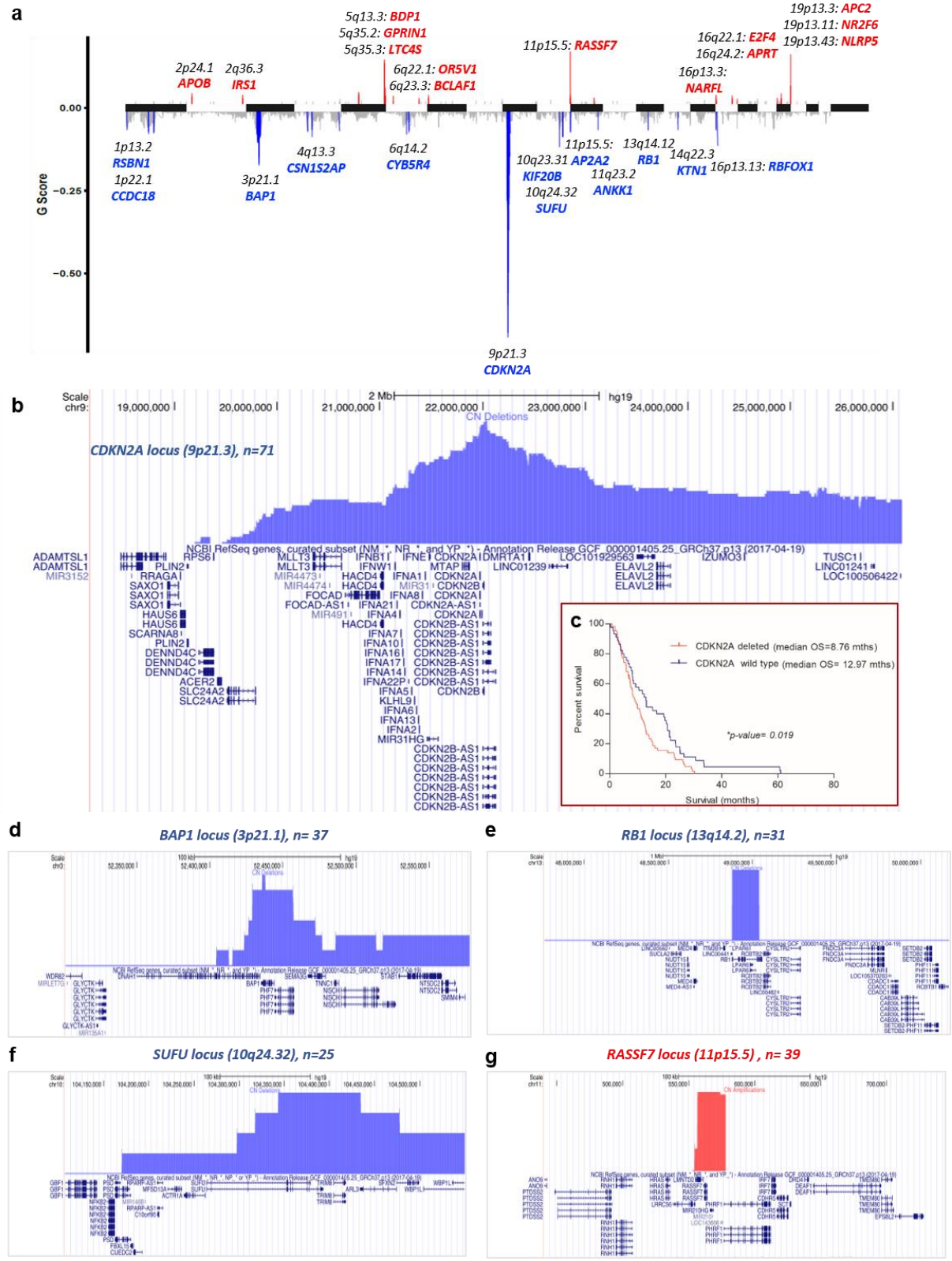

a) Statistically significant regions of amplification and deletion from GISTIC analysis of 118 subjects. Peak regions which pass both the G-Score (derived from amplitude and frequency) and q-bound (<0.05) threshold cut-offs are shown for deletions (blue) and amplifications (red) (see also Extended Data: Table 2); b) Detailed map of the *CDKN2A* locus using the UCSC Genome Browser (hg19), showing histogram representation of overlap among deletion segments from the 118 subjects. *IFN* Type I genes are commonly within the deleted segments; c) Kaplan-Meier survival analysis of patients with and without *CDKN2A* locus deletions; d-f) Similar Genome Browser based maps of the *BAP1*, *RB1* and *SUFU* deleted segments; g) Map for amplification segments from the *RASSF7* locus.

Figure 2. Common genetic alterations in Malignant Pleural Mesothelioma

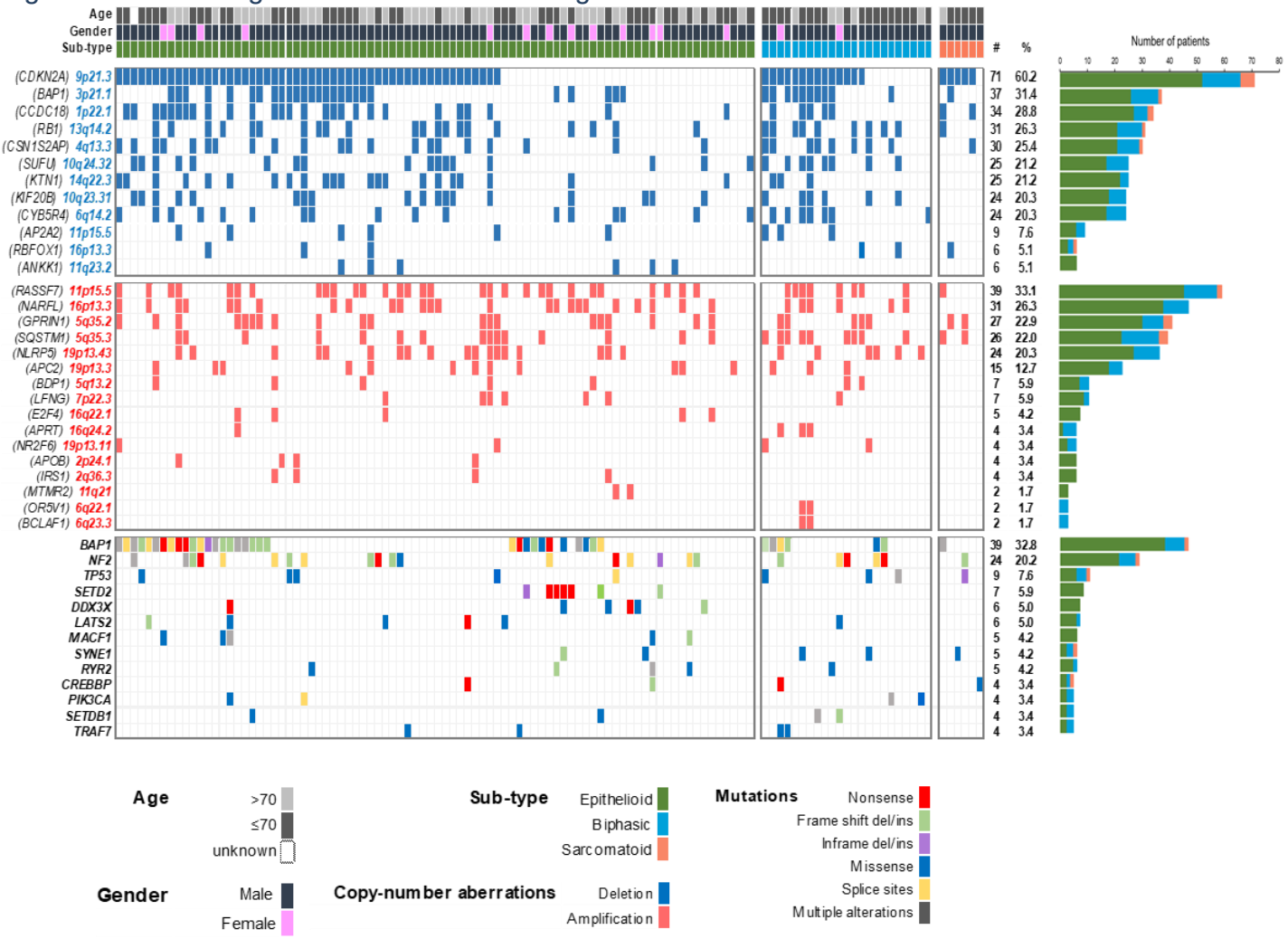

The most common deletions (top panel), amplifications (middle panel) and mutations (bottom panel) are shown in 118 subjects. CNA analyses are derived from SNP arrays and mutated genes from the targeted capture sequencing panel.

Figure 3. Response of cell lines to tested drugs

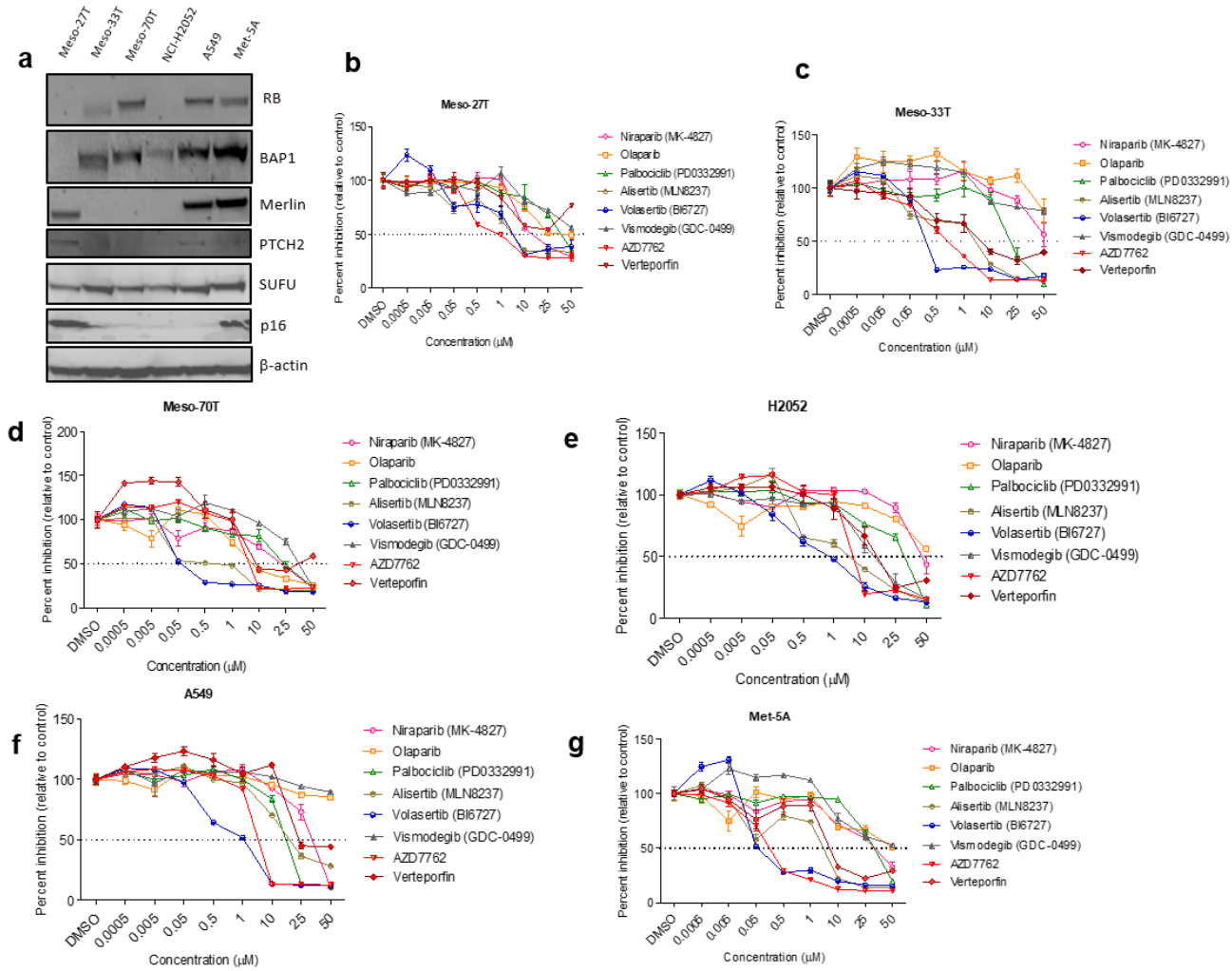

h

	DNA repair		Hedgehog	Hippo	Cell cycle RB1			
	Niraparib	Olaparib	Vismodegib	Verteporfin	Palbociclib	Alisertib	Volasertib	AZD7762
Cell line	PARP inhibitors		SMO inhibitor	YAP inhibitor	CDK4/6 inhibitor	Aurora kinase inhibitor	PLK1 inhibitor	CHEK1 inhibitor
Meso-27T	**7.96**	10.52	31.53	**1.08**	>50	**3.20**	**6.57**	**0.45**
Meso-33T	47.02	>50	**6.03**	**0.87**	20.29	**3.84**	**0.10**	**0.45**
Meso-70T	>50	**2.88**	>50	**1.2**	>50	**0.15**	**0.04**	**2.02**
NCI-H2052	29	27.3	13.7	10.9	>50	**0.81**	**0.64**	**2.42**
A549	>50	13.47	20.72	16.5	12.33	11.7	**0.71**	**1.84**
Met-5A	>50	11.13	**8.53**	**3.36**	29.2	>50	**0.44**	**0.11**

a) Characterisation by western blot of endogenous levels of RB, BAP1, Merlin (NF2), PTCH2, SUFU and p16 (CDKN2A) in primary cells and cell lines; b-g) Sensitivity dose curves for patient-derived MPM primary cells and cell lines against eight compounds. Standard errors of the mean are shown as bars. Dashed lines mark 50% inhibition; h) IC_{50} values for responses normalized to the control (DMSO), calculated by fitting a dose-response curve model in Graph Pad Prism and tabulated as concentration of drugs in µM. In cases where responses were above the highest drug concentration used in the experiment, IC_{50} estimates are marked as >50µM. Values in bold depict sensitive primary cells and cell lines, where IC_{50} to compounds <10µM and R^2 (goodness of fit of curve) >0.7.

References

[1] Disselhorst, M.J. *et al.*, Ipilimumab and nivolumab in the treatment of recurrent malignant pleural mesothelioma (INITIATE): results of a prospective, single-arm, phase 2 trial. *The Lancet. Respiratory medicine* 7 (3), 260-270 (2019).

[2] Scherpereel, A. *et al.*, Nivolumab or nivolumab plus ipilimumab in patients with relapsed malignant pleural mesothelioma (IFCT-1501 MAPS2): a multicentre, open-label, randomised, non-comparative, phase 2 trial. *Lancet Oncol* 20 (2), 239-253 (2019).

[3] Upadhyay, D. & Kamp, D.W., Asbestos-induced pulmonary toxicity: role of DNA damage and apoptosis. *Exp Biol Med (Maywood)* 228 (6), 650-659 (2003).

[4] Odgerel, C.O. *et al.*, Estimation of the global burden of mesothelioma deaths from incomplete national mortality data. *Occup Environ Med* 74 (12), 851-858 (2017).

[5] van der Bij, S. *et al.*, Prognosis and prognostic factors of patients with mesothelioma: a population-based study. *Br J Cancer* 107 (1), 161-164 (2012).

[6] Bueno, R. *et al.*, Comprehensive genomic analysis of malignant pleural mesothelioma identifies recurrent mutations, gene fusions and splicing alterations. *Nat Genet* 48 (4), 407-416 (2016).

[7] Hmeljak, J. *et al.*, Integrative Molecular Characterization of Malignant Pleural Mesothelioma. *Cancer Discov* 8 (12), 1548-1565 (2018).

[8] Huret, J.L. *et al.*, Atlas of genetics and cytogenetics in oncology and haematology in 2013. *Nucleic Acids Res* 41 (Database issue), D920-924 (2013).

[9] Mermel, C.H. *et al.*, GISTIC2.0 facilitates sensitive and confident localization of the targets of focal somatic copy-number alteration in human cancers. *Genome Biol* 12 (4), R41 (2011).

[10] Yap, T.A., Aerts, J.G., Popat, S., & Fennell, D.A., Novel insights into mesothelioma biology and implications for therapy. *Nat Rev Cancer* 17 (8), 475-488 (2017).

[11] Felley-Bosco, E., Opitz, I., & Meerang, M., Hedgehog Signaling in Malignant Pleural Mesothelioma. *Genes (Basel)* 6 (3), 500-511 (2015).

[12] Lee, Y. *et al.*, Loss of suppressor-of-fused function promotes tumorigenesis. *Oncogene* 26 (44), 6442-6447 (2007).

[13] Volodko, N., Gordon, M., Salla, M., Ghazaleh, H.A., & Baksh, S., RASSF tumor suppressor gene family: biological functions and regulation. *FEBS Lett* 588 (16), 2671-2684 (2014).

[14] Zheng, X. *et al.*, The coiled-coil domain of oncogene RASSF 7 inhibits hippo signaling and promotes non-small cell lung cancer. *Oncotarget* 8 (45), 78734-78748 (2017).

[15] Okazaki, N., Takahashi, N., Kojima, S., Masuho, Y., & Koga, H., Protocadherin LKC, a new candidate for a tumor suppressor of colon and liver cancers, its association with contact inhibition of cell proliferation. *Carcinogenesis* 23 (7), 1139-1148 (2002).

[16] Islam, M.A., Sooro, M.A., & Zhang, P., Autophagic Regulation of p62 is Critical for Cancer Therapy. *Int J Mol Sci* 19 (5) (2018).

[17] Sy, S.M., Huen, M.S., & Chen, J., PALB2 is an integral component of the BRCA complex required for homologous recombination repair. *Proc Natl Acad Sci U S A* 106 (17), 7155-7160 (2009).

[18] Blokzijl, F., Janssen, R., van Boxtel, R., & Cuppen, E., MutationalPatterns: comprehensive genome-wide analysis of mutational processes. *Genome Medicine* 10 (1), 33 (2018).

[19] Alexandrov, L.B. *et al.*, Signatures of mutational processes in human cancer. *Nature* 500 (7463), 415-421 (2013).
[20] Chernova, T. *et al.*, Molecular profiling reveals primary mesothelioma cell lines recapitulate human disease. *Cell Death Differ* 23 (7), 1152-1164 (2016).
[21] Chernova, T. *et al.*, Long-Fiber Carbon Nanotubes Replicate Asbestos-Induced Mesothelioma with Disruption of the Tumor Suppressor Gene Cdkn2a (Ink4a/Arf). *Curr Biol* 27 (21), 3302-3314 e3306 (2017).
[22] Rehrauer, H. *et al.*, How asbestos drives the tissue towards tumors: YAP activation, macrophage and mesothelial precursor recruitment, RNA editing, and somatic mutations. *Oncogene* 37 (20), 2645-2659 (2018).
[23] Doi, M. *et al.*, Gpr176 is a Gz-linked orphan G-protein-coupled receptor that sets the pace of circadian behaviour. *Nat Commun* 7, 10583 (2016).
[24] Mateo, J. *et al.*, A decade of clinical development of PARP inhibitors in perspective. *Ann Oncol* (2019).
[25] Srinivasan, G. *et al.*, Synthetic lethality in malignant pleural mesothelioma with PARP1 inhibition. *Cancer Chemother Pharmacol* 80 (4), 861-867 (2017).
[26] Witkiewicz, A.K. *et al.*, Targeting the Vulnerability of RB Tumor Suppressor Loss in Triple-Negative Breast Cancer. *Cell Rep* 22 (5), 1185-1199 (2018).
[27] Romagnoli, S. *et al.*, Identification of potential therapeutic targets in malignant mesothelioma using cell-cycle gene expression analysis. *Am J Pathol* 174 (3), 762-770 (2009).
[28] Oser, M.G. *et al.*, Cells Lacking the RB1 Tumor Suppressor Gene Are Hyperdependent on Aurora B Kinase for Survival. *Cancer Discov* 9 (2), 230-247 (2019).
[29] Van den Bossche, J. *et al.*, In vitro study of the Polo-like kinase 1 inhibitor volasertib in non-small-cell lung cancer reveals a role for the tumor suppressor p53. *Mol Oncol* 13 (5), 1196-1213 (2019).
[30] Nakatani, K. *et al.*, Targeting the Hippo signalling pathway for cancer treatment. *J Biochem* 161 (3), 237-244 (2017).
[31] Woodard, G.A., Yang, Y.L., You, L., & Jablons, D.M., Drug development against the hippo pathway in mesothelioma. *Transl Lung Cancer Res* 6 (3), 335-342 (2017).
[32] Azzolin, L. *et al.*, YAP/TAZ incorporation in the beta-catenin destruction complex orchestrates the Wnt response. *Cell* 158 (1), 157-170 (2014).
[33] Kato, S. *et al.*, RET Aberrations in Diverse Cancers: Next-Generation Sequencing of 4,871 Patients. *Clin Cancer Res* 23 (8), 1988-1997 (2017).
[34] Nass, N. *et al.*, High neuronatin (NNAT) expression is associated with poor outcome in breast cancer. *Virchows Arch* 471 (1), 23-30 (2017).
[35] Ventii, K.H. *et al.*, BRCA1-associated protein-1 is a tumor suppressor that requires deubiquitinating activity and nuclear localization. *Cancer Res* 68 (17), 6953-6962 (2008).
[36] BLU-667 Controls RET-Altered Thyroid Cancers. *Cancer Discov* 9 (9), OF5 (2019).
[37] Meerang, M. *et al.*, Antagonizing the Hedgehog Pathway with Vismodegib Impairs Malignant Pleural Mesothelioma Growth In Vivo by Affecting Stroma. *Mol Cancer Ther* 15 (5), 1095-1105 (2016).
[38] Rowbotham, N.J. *et al.*, Activation of the Hedgehog signaling pathway in T-lineage cells inhibits TCR repertoire selection in the thymus and peripheral T-cell activation. *Blood* 109 (9), 3757-3766 (2007).
[39] de la Roche, M. *et al.*, Hedgehog signaling controls T cell killing at the immunological synapse. *Science* 342 (6163), 1247-1250 (2013).

[40] Lines, J.L. *et al.*, VISTA is an immune checkpoint molecule for human T cells. *Cancer Res* 74 (7), 1924-1932 (2014).
[41] Muller, S. *et al.*, V-domain Ig-containing suppressor of T-cell activation (VISTA), a potentially targetable immune checkpoint molecule, is highly expressed in epithelioid malignant pleural mesothelioma. *Mod Pathol* (2019).
[42] Borden, E.C., Interferons alpha and beta in cancer: therapeutic opportunities from new insights. *Nat Rev Drug Discov* 18 (3), 219-234 (2019).
[43] Liu, H. *et al.*, Tumor-derived IFN triggers chronic pathway agonism and sensitivity to ADAR loss. *Nat Med* 25 (1), 95-102 (2019).
[44] Ye, Z. *et al.*, Prevalent Homozygous Deletions of Type I Interferon and Defensin Genes in Human Cancers Associate with Immunotherapy Resistance. *Clin Cancer Res* 24 (14), 3299-3308 (2018).
[45] Christmas, T.I., Manning, L.S., Garlepp, M.J., Musk, A.W., & Robinson, B.W., Effect of interferon-alpha 2a on malignant mesothelioma. *J Interferon Res* 13 (1), 9-12 (1993).
[46] Sexl, V., Wagner, L., Wiesholzer, M., Presterl, E., & Base, W., Treatment of a patient with malignant mesothelioma with interferon-alpha 2 based on in vitro sensitivity tests. *Clin Investig* 72 (4), 317-320 (1994).
[47] Sterman, D.H. *et al.*, Pilot and Feasibility Trial Evaluating Immuno-Gene Therapy of Malignant Mesothelioma Using Intrapleural Delivery of Adenovirus-IFNalpha Combined with Chemotherapy. *Clin Cancer Res* 22 (15), 3791-3800 (2016).
[48] Sterman, D.H. *et al.*, A phase I trial of repeated intrapleural adenoviral-mediated interferon-beta gene transfer for mesothelioma and metastatic pleural effusions. *Mol Ther* 18 (4), 852-860 (2010).
[49] Leiserson, M.D. *et al.*, Pan-cancer network analysis identifies combinations of rare somatic mutations across pathways and protein complexes. *Nat Genet* 47 (2), 106-114 (2015).
[50] McLaren, W. *et al.*, The Ensembl Variant Effect Predictor. *Genome Biol* 17 (1), 122 (2016).
[51] Jian, X., Boerwinkle, E., & Liu, X., In silico prediction of splice-altering single nucleotide variants in the human genome. *Nucleic Acids Res* 42 (22), 13534-13544 (2014).
[52] Blokzijl, F., Janssen, R., van Boxtel, R., & Cuppen, E., MutationalPatterns: comprehensive genome-wide analysis of mutational processes. *Genome Med* 10 (1), 33 (2018).

Genomic mapping identifies multiple therapeutic pathways in malignant mesothelioma

EXTENDED DATA

Anca Nastase[1¶], Amit Mandal[1¶], Shir Kiong Lu[1], Hima Anbunathan[1], Deborah Morris-Rosendahl[1,2], Yu Zhi Zhang[1,3], Xiao-Ming Sun[4], Spyridon Gennatas[1], Robert C Rintoul[5,6], Matthew Edwards[2], Alex Bowman[3], Tatyana Chernova[4], Tim Benepal[7], Eric Lim[8], Anthony Newman Taylor[1], Andrew G Nicholson[1,3], Sanjay Popat[9,10], Anne E Willis[4], Marion MacFarlane[4], Mark Lathrop[11], Anne M Bowcock[1], Miriam F Moffatt[1,*], William OCM Cookson[1,*]

Contents

Extended Data Table 1. Patient demographics 2
Extended Data Table 2. Significant copy number deletions and amplifications 3
Extended Data Table 3. Targeted sequencing gene panel 4
Extended Data Table 4. Genes differentially regulated in histological subtypes 5
Extended Data Table 5. Correlation of *SUFU* and immune function genes and replication 6
Extended Data Table 6. Genes differentially up-regulated in *BAP1* mutated tumours 7
Extended Data Figure 1. Analytical structure 8
Extended Data Figure 2. Oncoplot from targeted sequencing panel 9
Extended Data Figure 3. Mutation characteristics 10
Extended Data Figure 4. Histologic features of MPM 11

Extended Data Table 1. Patient demographics

	Group					
	Whole Exome Sequencing (n=50)	**SNP genotyping (n=118)**	**Targeted Capture Sequencing (n=119)**	**RNA sequencing (n=35)**	**IHC (n=28)**	**All (n=121)**
Gender (n, %)						
M	39 (78.0)	103 (87.3)	103 (86.6)	25 (75.8)	23 (82.1)	105 (86.8)
F	11 (22.0)	15 (12.7)	16 (13.4)	8 (24.2)	5 (17.9)	16 (13.2)
M:F	3.5:1	6.9:1	6.4:1	3.13:1	4.6:1	6.6:1
Age						
Average ± SD	69.7 ± 8.2	72.1 ±8.5	72.1 ± 8.5	70.06 ± 8.3	67.6 ± 8.1	72.1 ± 8.4
median [range]	69.7 [52-90]	73.0 [51-90]	72.6 [51-90]	69.0 [55-90]	67 [52-82]	73 [51-90]
Histology (n, %)						
Epithelioid	34 (68.0)	89 (75.4)	88 (74.0)	26 (74.3)	19 (67.9)	90 (74.4)
Biphasic	14 (28.0)	23 (19.5)	25 (21.0)	6 (17.1)	9 (32.1)	25 (20.6)
Sarcomatoid	2 (4.0)	6 (5.1)	6 (5.0)	3 (8.6)	0 (0.0)	6 (5.0)
Overall survival						
Data available	92.0%	91.5%	92.4%	85.7%	100.0%	
All (months, [rate at 12 months])	9.93 [42.63%]	9.93 [42.24%]	9.93 [42.39%]	10.43 [43.75%]	12.8 [59.74%]	9.93 [42.0%]
Epithelioid	10.43 [45.16%]	11.6 [48.75%]	11.6 [48.75%]	12.27 [52.17%]	12.96 [68.42]	11.6 [48.15%]
Biphasic	10.86 [42.73%]	7.4 [29.54%]	7.4 [31.41%]	7.07 [33.33%]	10.87 [38.1%]	7.4 [31.41%]
Sarcomatoid	1.5 [0.0%]	3.66 [0.0%]	3.66 [0.0%]	1.5 [0.0%]	NA	3.67 [0.0%]
Asbestos exposure (n, %)						
Yes	32 (64.0)	63 (68.5)	63 (67.7)	20 (57.1)	21 (75.0)	83 (68.6)
No	16 (32.0)	27 (29.3)	28 (30.1)	11 (31.4)	6 (21.4)	36 (29.8)
Unknown	2 (4.0)	2 (2.2)	2 (2.2)	4 (11.4)	1 (3.6)	2 (1.6)

Extended Data Table 2. Significant copy number deletions and amplifications

DELETIONS					
cytoband	**q value**	**residual q**	**wide peak boundaries**	**Kb**	**Principal Genes**
9p21.3	2.4E-112	2.4E-112	chr9:21927328-22031004	104	*CDKN2A, CDKN2B, 9orf53*
3p21.1	7.3E-10	7.3E-10	chr3:52433746-52449046	15	*BAP1*
10q23.31	8.6E-05	1.6E-04	chr10:91440057-91589280	149	*KIF20B, FLJ37201*
16p13.3	1.6E-04	1.4E-03	chr16:5128784-7773249	2644	*RBFOX1, FAM86A*
4q13.3	2.2E-03	3.2E-03	chr4:70932306-71062425	130	*CSN1S2AP, C4orf40, CSN1S2BP*
6q14.2	5.8E-03	5.5E-03	chr6:84563880-84759646	196	*CYB5R4*
11p15.5	1.6E-02	1.6E-02	chr11:906709-1083236	177	*AP2A2, MUC6*
10q24.32	2.5E-03	2.7E-02	chr10:104245589-104485300	240	*ARL3, SUFU, TRIM8*
1p22.1	7.5E-03	3.9E-02	chr1:93620394-93787866	167	*CCDC18*
13q14.2	4.2E-02	4.2E-02	chr13:48835311-49063155	228	*RB1, LPAR6*
11q23.2	4.7E-02	4.9E-02	chr11:113236976-113280927	44	*ANKK1*
14q22.3	4.8E-02	4.9E-02	chr14:56023823-56271005	247	*KTN1, RPL13AP3, LINC00520, KTN1-AS1*
AMPLIFICATIONS					
cytoband	**q value**	**residual q**	**wide peak boundaries**	**Kb**	**Principal Genes**
11p15.5	6.4E-48	6.4E-48	chr11:552679-587371	35	*RASSF7, PHRF1, LRRC56, LOC143666, C11orf35, MIR210, MIR210HG*
19q13.43	6.1E-45	6.1E-45	chr19:56572845-56674547	102	*ZNF444, NLRP5, ZNF787*
5q35.2	3.8E-39	1.2E-37	chr5:176025071-176043332	18	*GPRIN1*
5q35.3	1.8E-10	8.3E-08	chr5:179214819-179249072	34	*LTC4S, SQSTM1, MGAT4B, MIR1229*
2p24.1	9.1E-06	9.1E-06	chr2:21210344-21227220	17	*APOB*
19p13.11	9.1E-06	9.1E-06	chr19:17339697-17370189	30	*NR2F6, OCEL1, USHBP1*
7p22.3	1.2E-04	1.2E-04	chr7:2552807-2579466	27	*LFNG, BRAT1, MIR4648*
16p13.3	1.2E-04	1.2E-04	chr16:772127-786320	14	*NARFL, FAM173A, HAGHL, CCDC78*
2q36.3	1.6E-04	1.6E-04	chr2:227646960-227686906	40	*IRS1*
16q22.1	2.7E-04	2.7E-04	chr16:67220742-67229485	9	*E2F4, EXOC3L1*
6p22.1	6.9E-04	6.9E-04	chr6:29311440-29325601	14	*OR5V1*
5q13.2	1.5E-06	4.7E-03	chr5:70806522-70855825	49	*BDP1*
11q21	1.8E-02	1.8E-02	chr11:95569326-95603081	34	*MTMR2*

6q23.3	2.2E-02	2.2E-02	chr6:136582550-136648626	66	*BCLAF1*
19p13.3	2.2E-02	2.2E-02	chr19:1457003-1482901	26	*APC2, PCSK4, C19orf25*
16q24.2	4.6E-02	4.6E-02	chr16:88498491-89347394	849	*APRT, CBFA2T3, CDH15, CYBA, GALNS, MVD, PIEZO1, IL17C, ANKRD11, TRAPPC2L, CDT1, ZNF469, RNF166, ZC3H18, SLC22A31, ZFPM1, MGC23284, ZNF778, ACSF3, LINC00304, SNAI3, CTU2, PABPN1L, LOC400558, MIR4722*

Extended Data Table 3. Targeted sequencing gene panel

ANKLE1	*CDKN2A*	*FOXD1*	*MAML3*	*NF2*	*SETD1B*	*TJP2*	*ZNF880*
APC	*CFAP45*	*HERC1*	*MLH1*	*NRAS*	*SETD2*	*TJP3*	
ASS1	*CREBBP*	*HERC2*	*MMP17*	*PIK3CA*	*SETD6*	*TP53*	
ATXN2	*DDX3X*	*ICA1*	*MSH2*	*PRDM12*	*SETDB1*	*TRAF7*	
BAP1	*DDX51*	*INADL*	*MSH3*	*PRKRA*	*SF3B1*	*ULK2*	
BRCA2	*EGFR*	*LATS1*	*MSH5*	*PTEN*	*SLC2A3*	*VEZF1*	
BRD4	*EP400*	*LATS2*	*MSH6*	*RB1*	*SYNE1*	*WDR89*	
CD163	*FBXW7*	*MACF1*	*NCOR2*	*RYR2*	*TET1*	*ZNF77*	

Extended Data Table 4. Genes differentially regulated in histological subtypes

Log2 Fold Change	Average Expression	Adjusted P Value	Chr	Name	Description
5.23	-2.62	2.10E-04	7	*NFE4*	Nuclear factor in erythrogenesis
4.72	-0.21	1.90E-04	3	*RP4-555D20.2*	miRNA
4.65	-1.60	9.13E-04	17	*IGF2BP1*	Novel interacting partner of p38 MAPK. RNA-binding protein, involved in tumour progression
4.50	-0.31	9.13E-04	5	*GDNF*	Glial cell derived neurotrophic factor
3.66	1.57	9.92E-04	18	*CCBE1*	High levels contribute to aggressiveness and poor prognosis of Colon Cancer
3.57	3.41	7.26E-04	12	*WNT5B*	Activator of WNT signalling
3.45	-2.82	9.13E-04	15	*CTD-2033D15.2*	Non-coding cDNA
3.33	-3.95	9.91E-04	3	*RP4-555D20.4*	miRNA
2.89	-3.88	7.18E-04	X	*RP11-320G24.1*	miRNA
2.66	1.29	7.26E-04	17	*HS3ST3A1*	Tumour regulator and prognostic marker in breast cancer.
2.27	5.55	2.10E-04	1	*NAV1*	Potentiates migration of breast cancer cells
2.25	3.73	7.26E-04	2	*CHN1*	Actin dynamics in cell migration
2.15	3.41	7.26E-04	15	*GPR176*	Orphan G-protein-coupled receptor that sets the pace of circadian behaviour
1.95	6.25	2.58E-04	4	*SEPT11*	
1.73	5.81	9.57E-04	6	*TRAM2*	Putative metastatic factor for oral cancer
1.50	3.88	9.57E-04	2	*SERTAD2*	Promotes oncogenesis in nude mice and is frequently overexpressed in multiple human tumours.

Genes differentially up-regulated in sarcomatoid and mixed histology compared to epithelioid. Transcripts with average expression ≥ 1 are shown. *P* values are adjusted for multiple comparisons (false discovery rate <0.05).

Extended Data Table 5. Correlation of *SUFU* and immune function genes and replication

NCMR n=35	***SUFU***		***PTCH2***		***PTCH1***		***CR1***		***KLRD1***		***PD-L1***	
PTCH2	-0.38	*2.5E-02*										
PTCH1	-0.37	*3.1E-02*	0.75	*1.7E-07*								
CR1	0.50	*2.2E-03*	-0.59	*1.8E-04*	-0.41	*1.4E-02*						
KLRD1	0.37	*2.9E-02*	-0.60	*1.4E-04*	-0.52	*1.3E-03*	0.56	*5.1E-04*				
PD-L1	0.10	*5.8E-01*	-0.39	*2.2E-02*	-0.44	*8.1E-03*	0.35	*4.1E-02*	0.37	*2.8E-02*		
VISTA	0.61	*1.1E-04*	-0.52	*1.3E-03*	-0.41	*1.3E-02*	0.43	*1.0E-02*	0.68	*7.5E-06*	0.09	*6.1E-01*
TGCA-Meso n=86												
PTCH2	-0.08	*4.6E-01*										
PTCH1	0.09	*3.9E-01*	0.77	*2.2E-16*								
CR1	-0.04	*7.1E-01*	-0.09	*4.1E-01*	-0.11	*3.4E-01*						
KLRD1	-0.04	*7.0E-01*	-0.36	*6.2E-04*	-0.33	*1.9E-03*	0.41	*7.9E-05*				
PD-L1	-0.26	*1.7E-02*	-0.22	*4.0E-02*	-0.30	*5.5E-03*	0.35	*8.1E-04*	0.40	*1.7E-04*		
VISTA	0.25	*2.1E-02*	-0.47	*5.9E-06*	-0.25	*2.2E-02*	-0.06	*5.9E-01*	0.37	*4.8E-04*	-0.09	*4.0E-01*
Bueno *et al*. n=211												
PTCH2	-0.22	*1.4E-03*										
PTCH1	-0.16	*1.8E-02*	0.71	*2.2E-16*								
CR1	0.30	*9.6E-06*	-0.20	*2.9E-03*	-0.23	*7.9E-04*						
KLRD1	0.26	*1.1E-04*	-0.37	*3.1E-08*	-0.35	*2.4E-07*	0.49	*7.1E-14*				
PD-L1	-0.08	*2.3E-01*	-0.16	*1.7E-02*	-0.31	*6.0E-06*	0.42	*2.8E-10*	0.38	*1.2E-08*		
VISTA	0.27	*5.6E-05*	-0.36	*6.0E-08*	-0.27	*8.3E-05*	0.06	*3.9E-01*	0.36	*6.8E-08*	-0.06	*3.5E-01*
Combined studies												
PTCH2	-0.21	*9.96E-05*										
PTCH1	-0.14	*1.20E-02*	0.73	*<2.2E-16*								
CR1	0.16	*3.53E-03*	-0.17	*2.23E-03*	-0.15	*6.87E-03*						
KLRD1	0.14	*9.81E-03*	-0.33	*6.71E-10*	-0.28	*3.33E-07*	0.55	*<2.2E-16*				
PD-L1	-0.09	*8.96E-02*	-0.18	*7.87E-04*	-0.28	*3.31E-07*	0.42	*1.78E-15*	0.42	*1.33E-15*		
VISTA	0.33	*6.93E-10*	-0.42	*2.00E-15*	-0.32	*3.81E-09*	-0.06	*2.66E-01*	0.22	*5.59E-05*	-0.11	*5.50E-02*

Pearson correlations between abundances of Hedgehog pathway transcripts *SUFU*, *PTCH1*, *PTCH2* and transcripts related to immune checkpoints. The official gene names for PD-L1 and VISTA are *CD274* and *VSIR*, respectively. Results are shown for the present study, two previous investigations and for all studies combined. Two sided-*P* values are shown in italics throughout.

Extended Data Table 6. Genes differentially up-regulated in *BAP1* mutated tumours

Log2 Fold Change	Average Expression	Adjusted P Value	Chr	Name	Description
6.09	4.33	1.88E-02	20	*NNAT*	Marker of poor outcome in many cancers
3.60	1.47	7.77E-03	16	*NECAB2*	Neuronal calcium-binding protein that binds to adenosine A(2A) and metabotropic glutamate type 5 receptors
3.20	3.51	4.77E-02	22	*TAFA5*	Postulated to function as brain-specific chemokine or neurokine
2.70	2.43	1.88E-02	21	*PDE9A*	Phosphodiesterase 9A
2.36	1.68	4.77E-02	10	*RET*	Tyrosine kinase receptor leading to oncogenic signalling that is targetable with anti-RET multikinase inhibitors
1.85	4.08	4.77E-02	19	*HSD17B14*	Hydroxysteroid 17-beta dehydrogenase 14

Extended Data Figure 1. Analytical structure

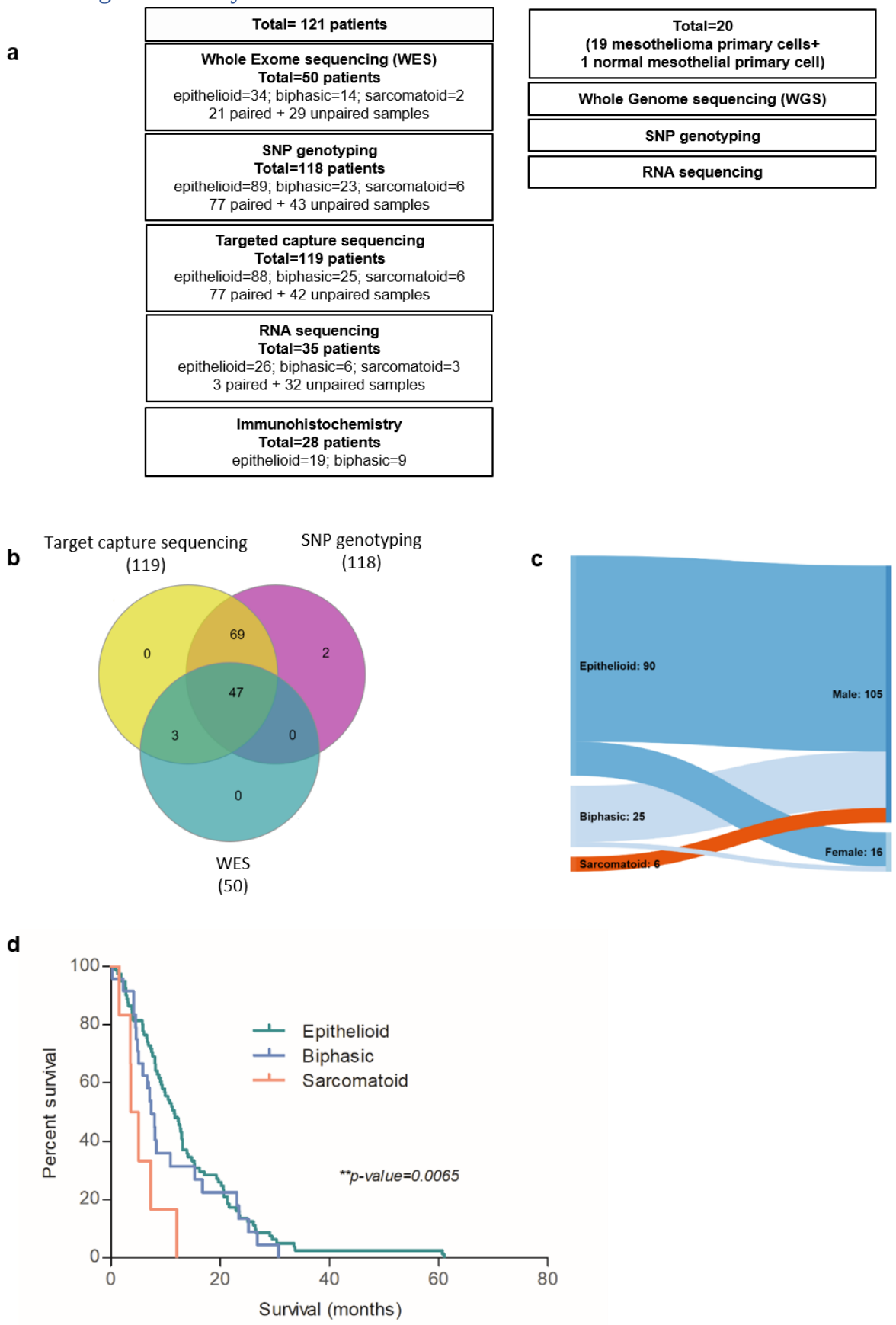

a) Summary of samples used in each analysis; b) Venn diagram showing overlapping of samples used in WES, SNP genotyping and targeted capture sequencing; c) Sankey diagram on histological subtype and patients` gender; d) Kaplan-Meier survival curves on histological subtypes

Extended Data Figure 2. Oncoplot from targeted sequencing panel

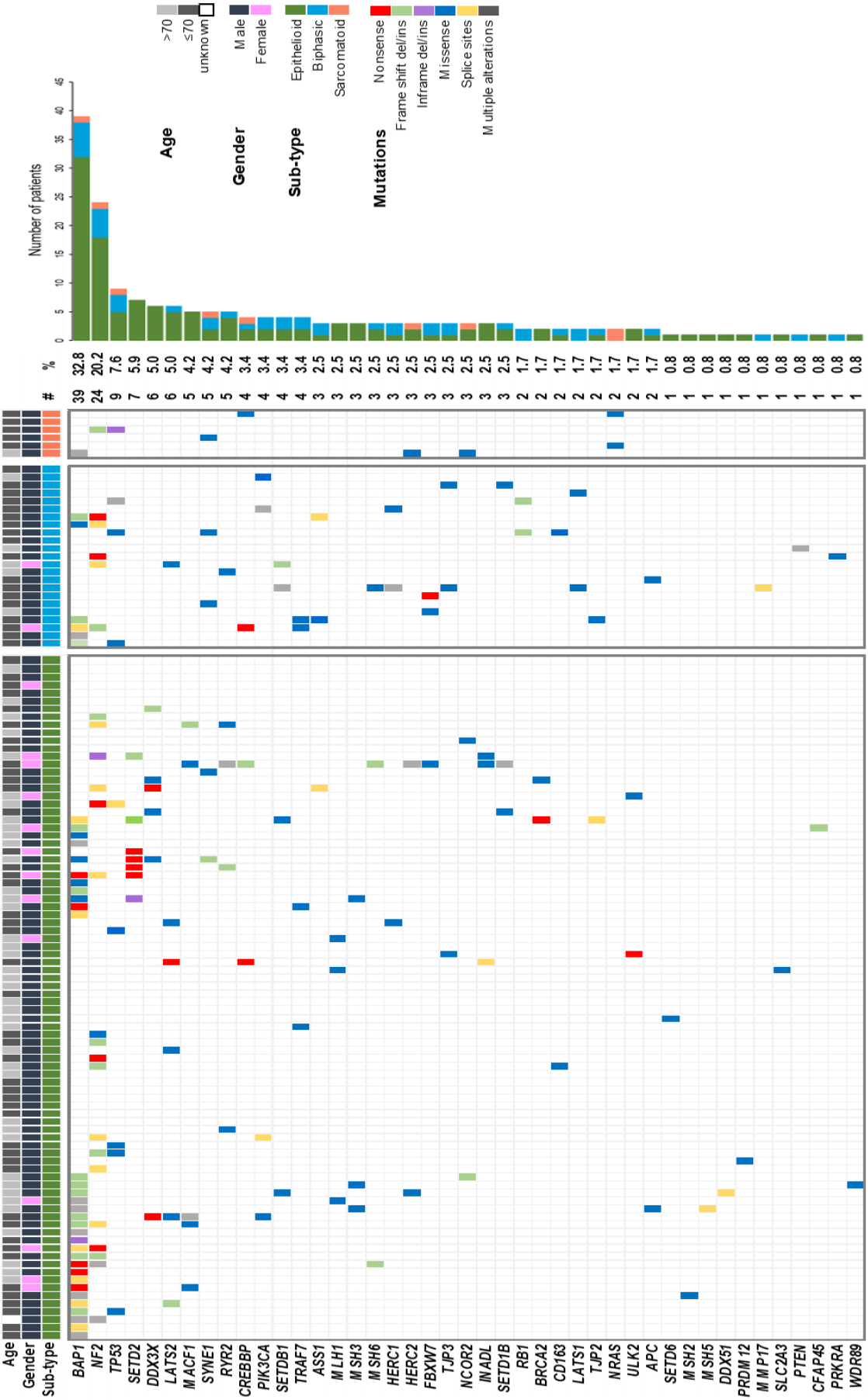

Extended Data Figure 3. Mutation characteristics

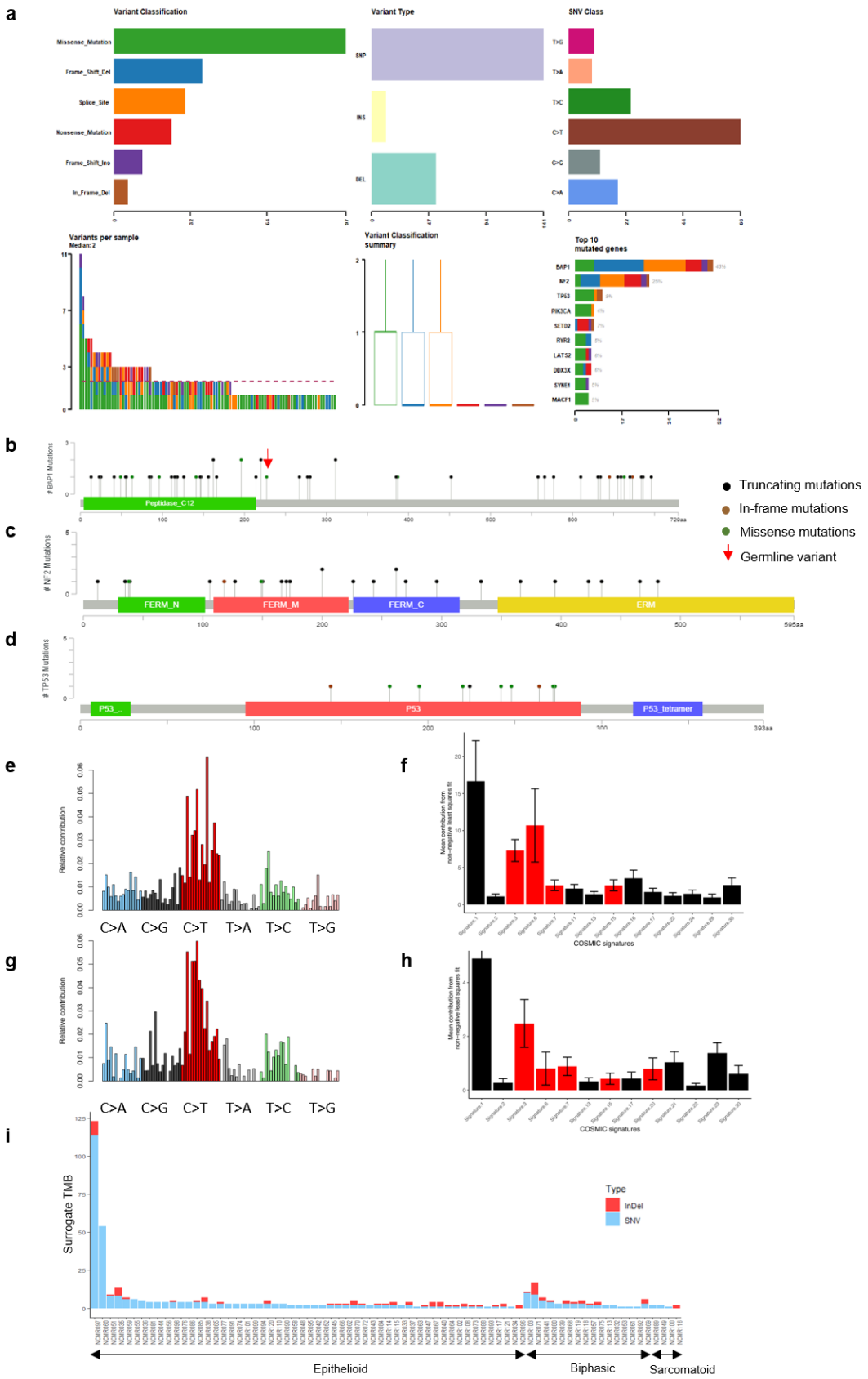

a) Summary of mutation spectrum observed for genes from targeted capture sequencing panel; b-d) Distribution of mutations in *BAP1*, *NF2*, and *TP53*; e) Mutational signature in 21 paired MPM analysed by WES; f) Mean percentage of contribution for COSMIC signatures; g) Mutational signature in 19 patient-derived MPM cell lines; h) Mean percentage COSMIC signatures in each cell line; i) Tumour mutation burden (TMB) derived from targeted capture sequencing of 57-gene panel and hence abbreviated as 'Surrogate TMB', in 77 paired samples. Briefly, all somatic SNVs or, InDels observed per sample, across the gene-panel are summed to derive surrogate TMB.

Extended Data Figure 4. Histologic features of MPM

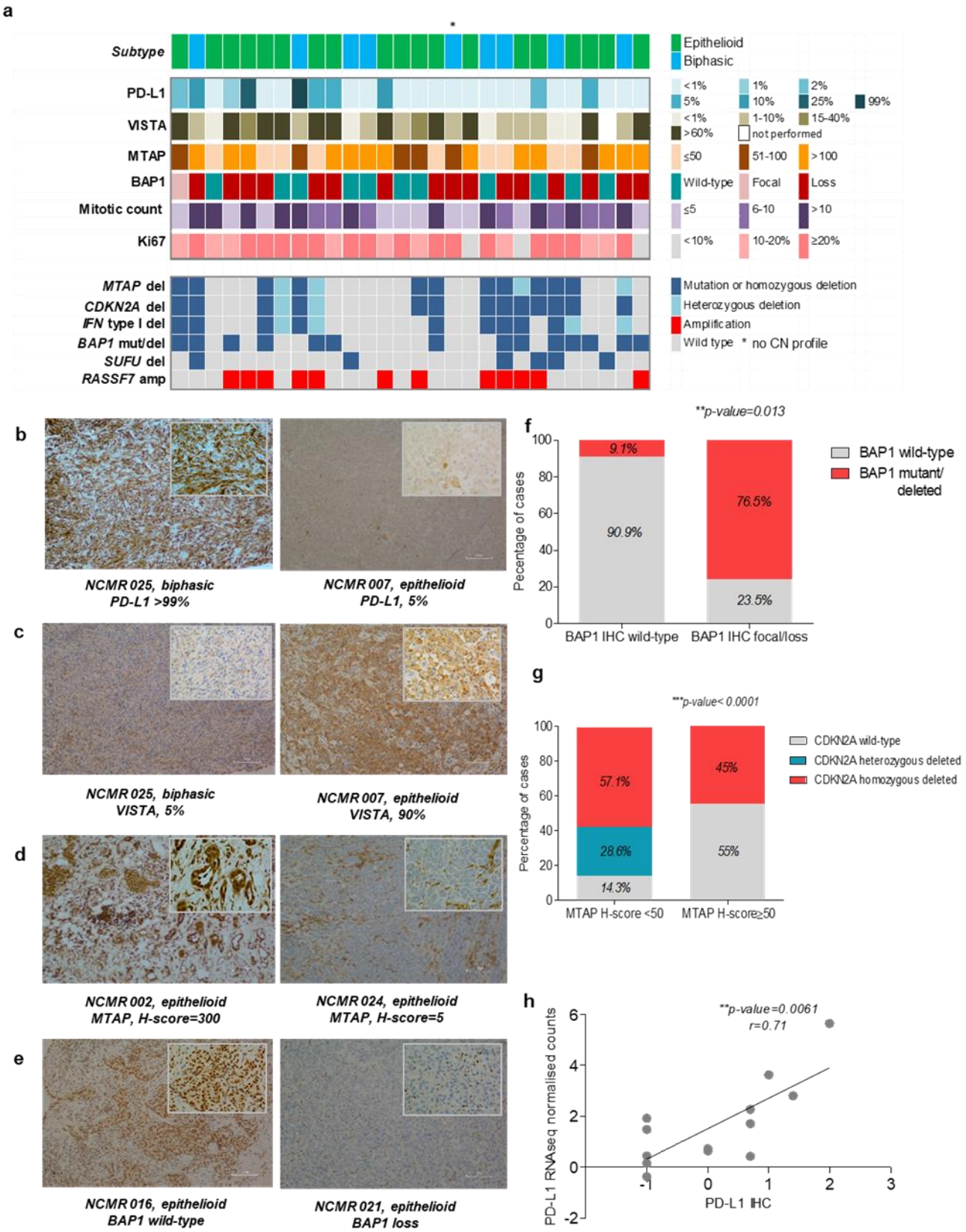

a) Oncoplot of IHC staining and common genomic alterations; b-e) representative IHC images for PD-L1, VISTA, MTAP and BAP1 (100x and 400x) ; f) Analysis on BAP1 genomic and proteomic status by Fisher`s exact test; g) Analysis of MTAP H-score in *CDKN2A/MTAP* deleted vs *CDKN2A/MTAP* wild-type by Fisher`s exact test, with a threshold for MTAP H-score set at 50; h) Spearman correlation between PD-L1 gene expression and IHC.